Journal of ELECTRONIC MATERIALS, Vol. 46, No. 1, 2017
DOI: 10.1007/s11664-016-4842-5

Dielectric, Impedance and Conduction Behavior of Double Perovskite Pr_2CuTiO_6 Ceramics

DEV K. MAHATO[1,3] and T.P. SINHA[2]

1.—Department of Physics, National Institute of Technology Patna, Patna 800 005, India. 2.—Department of Physics, Bose Institute, 93/1, Acharya Prafulla Chandra Road, Kolkata 700 009, India. 3.—e-mail: drdevkumar@yahoo.com

Polycrystalline Pr_2CuTiO_6 (PCT) ceramics exhibits dielectric, impedance and modulus characteristics as a possible material for microelectronic devices. PCT was synthesized through the standard solid-state reaction method. The dielectric permittivity, impedance and electric modulus of PCT have been studied in a wide frequency (100 Hz–1 MHz) and temperature (303–593 K) range. Structural analysis of the compound revealed a monoclinic phase at room temperature. Complex impedance Cole–Cole plots are used to interpret the relaxation mechanism, and grain boundary contributions towards conductivity have been estimated. From electrical modulus formalism polarization and conductivity relaxation behavior in PCT have been discussed. Normalization of the imaginary part of impedance (Z'') and the normalized imaginary part of modulus (M'') indicates contributions from both long-range and localized relaxation effects. The grain boundary resistance along with their relaxation frequencies are plotted in the form of an Arrhenius plot with activation energy 0.45 eV and 0.46 eV, respectively. The ac conductivity mechanism has been discussed.

Key words: Double perovskite, x-ray diffraction, conductivity, electrical properties

INTRODUCTION

Due to technological advancements, new electronic devices require materials with multiple features and high performance. Titanate-related material $CaCu_3Ti_4O_{12}$ has attracted the interest of researchers during the last few years due to its high temperature-independent (100–400 K) and frequency-independent (up to 10 MHz) dielectric constant ($\varepsilon_r \sim 10^{4-5}$), which is desirable in microelectronic devices such as capacitors and memory devices. The TiO_2 compound thin film stands out as an important material for many applications such as protection, decoration and fabrication of optoelectronic devices, and its ceramic compositions can compete with metal topologies in near-antenna filters in base stations.[1] It also shows interesting optical applications in view of its high transmission over a wide spectral range and other interesting characteristics such as its high refractive index and band gap.[2] The high value of dielectric constants have been observed in various materials[3–5] including double perovskites.[6,7] Double perovskite oxides $A_2BB'O_6$ have become candidates of growing interest due to their possible applications in non-volatile magnetic random access memory, magnetic sensors, magnetic read heads for hard drives, superconductors, relaxers, photonics, catalysts and a multitude of microelectronics and telecommunications, etc. The $A_2BB'O_6$ are derived from the ABO_3 perovskites, when half of the octahedral-coordinated B-site cations are replaced by appropriate B′ cations.[8] Usually, A is a large cation (rare earth or alkaline earth metal) while B and B′ correspond to smaller heterovalent cations (d-block transition metal). Due to non-ideal A-O and B-O bond distances and distorted lattice symmetries, double perovskites can be used as dielectric resonators and filters to store and transfer

(Received February 16, 2016; accepted July 30, 2016; published online August 17, 2016)

microwave communication signals and have great application in cellular communication industry.[1,9] Currently, extensive experimental and theoretical studies are still being carried out to search for $A_2BB'O_6$ materials with optimized properties. In recent years, interest has grown in the technological properties of double perovskites made of a mixture of rare earth metals and transition metal elements. These systems are characterized by their flexibility to develop new materials with improved properties. In the last few years, a large number of structural, electric and magnetic properties of double perovskite analogues of A_2CuTiO_6 (A = Y, Tb-Lu,[10] Y, Dy, Ho, Eu and Yb,[11,12] La[13–15]) have been systematically investigated, while a detailed literature survey shows that the A = Pr-based analogues have not been studied in similar detail, although the ionic radius of Pr^{3+} is very close to that of La^{3+}, Eu^{3+}, Ho^{3+} , etc. Pr^{3+}, one of the largest of the lanthanides, has the only 3+ ion considered and Pr is valued for its magnetic, electrical, chemical, and optical properties, and Cu and Ti are rich with electrical nature. The mixed valence structure (Cu^{+}/Cu^{2+} and Ti^{3+}/Ti^{4+}) found in La_2CuTiO_6 and $CaCu_3Ti_4O_{12}0$ may lead to the similar optimised electrical properties in a new $Pr_{20}CuTiO_6$.

In this context, we, therefore, propose to develop the double perovskite with rare earth ions (Pr^{3+}) at the A-site and transition metal ions (Cu^{2+} and Ti^{+4}) atthe B-site of the structure, and investigate their dielectric, electrical and conduction properties by impedance spectroscopy in the frequency range 100 Hz–1 MHz and in the temperature range 303–593 K.

EXPERIMENTAL

Materials and Methods

The Pr_2CuTiO_6 (PCT) ceramic specimens have been prepared by the multi-step mixed oxide route. High-purity powders of Pr_2O_3, CuO and TiO_2 were used as starting materials and thoroughly mixed in a stoichiometric ratio in an agate mortar in the presence of acetone (MERCK) for 10 h. The mixture was calcined in a Pt crucible at 1373 K in air for 10 h. The calcined powder was crushed thoroughly and pelletized into a circular disk (thickness of 2 mm and diameter of 8 mm) using polyvinyl alcohol as a binder. Finally, the disks were sintered at 1473 K at a heating rate of 2°C/min and maintained at this temperature for 6 h and then cooled down to room temperature by adjusting the cooling rate.

Characterization

The phase formation was confirmed by x-ray diffraction (XRD) studies using an x-ray powder diffractometer (Rigaku Miniflex-II). The x-ray diffractogram of the sample was collected in a wide range of Bragg angles ($20° \le 2\theta \le 80°$) using Cu$K\alpha$ radiation (λ = 1.5418 Å) and a Ni filter operating at 40 kV and 20 mA at a scanning rate of 2°/min. The microstructure and the grain size distribution of the sintered pellets were studied using a scanning electron microscope (FEI Quanta 200). For the electric characterization, the sintered disk was polished, then coated with a conducting high-purity ultrafine silver paste for making electrical contacts. The disk was dried at 473 K for 30 min. The dielectric measurements and impedance measurements were carried out using an inductance capacitance resistance (LCR) meter (computer interfaced HIOKI 3532-50 LCR Hitester) from 100 Hz to 1 MHz and in the temperature range of 303–593 K.

RESULTS AND DISCUSSION

Structural Study

Figure 1 shows an XRD pattern of the PCT sample recorded at room temperature. All the peaks of the x-ray profile were indexed taking their 2θ values, and lattice parameters were determined by using the standard computer program. Good agreement between the observed and calculated interplanar spacing (d values) suggests the compound has a monoclinic structure at room temperature with lattice parameters a = 7.753486 Å ± 0.002915 Å; b = 3.931478 Å ± 0.000838 Å; c = 7.331871 Å ± 0.002549 Å; β = 97.591960° ± 0.036608° and unit cell volume V = 221.54 Å^3. All the peaks were observed in the range of $18° < 2\theta < 81°$ and no impurity phase was identified, indicating that the solid-state reaction method allows a single perovskite phase to be obtained. The scanning electron microscopy (SEM) picture of PCT is shown in the inset of Fig. 1. It is clear that grain sizes are widely distributed from submicrons to 1.4 μm with irregularly shaped grains.

Dielectric Study

The dielectric features of a material are usually described by its permittivity and its dielectric loss.

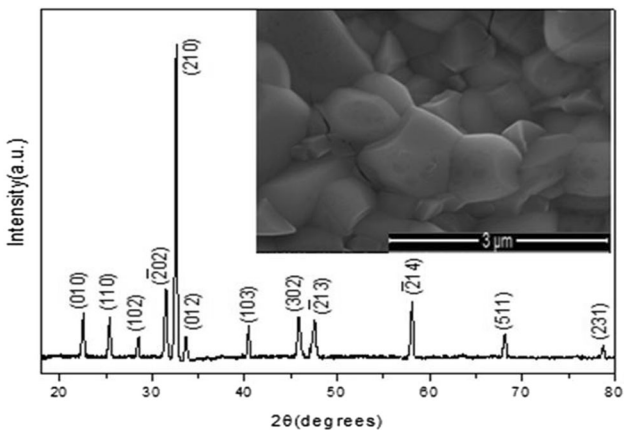

Fig. 1. Room temperature XRD and SEM (inset) of Pr_2CuTiO_6.

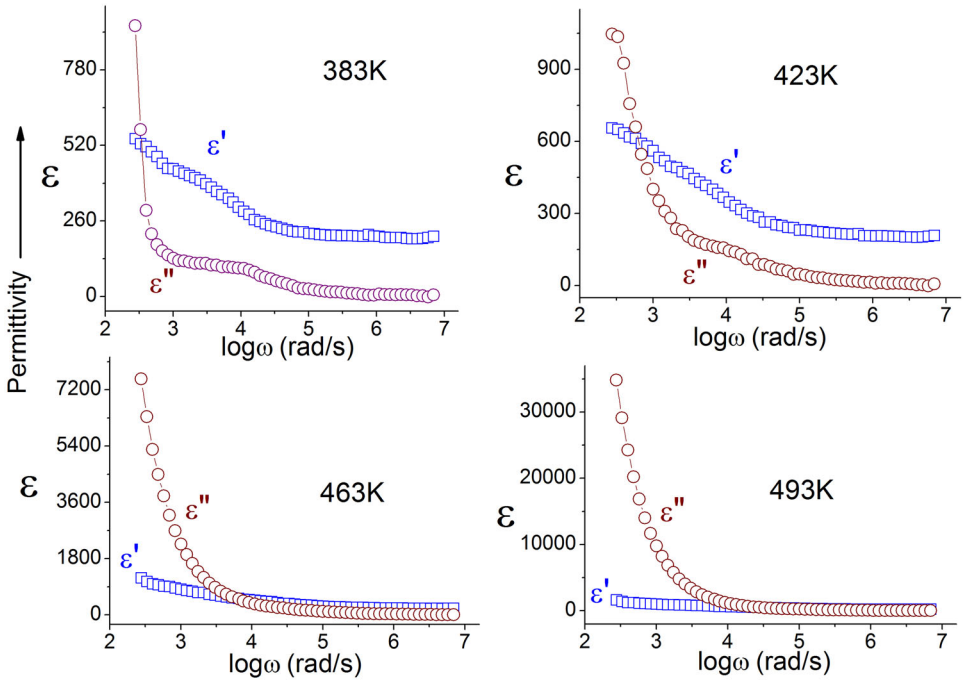

Fig. 2. Variation of real and imaginary dielectric constants as a function of frequency at various temperatures of Pr_2CuTiO_6.

The complex dielectric permittivity $\varepsilon = \varepsilon' + i\varepsilon''$ characterizes the electrical properties of PCT ceramics, where ε' is the real part, and ε'' is the imaginary part of dielectric constant. The real part is the measure of the polarizability of the material. The imaginary part reflects the dissipative loss in the material.[16] The variation of ε' and ε'' with frequency at different temperatures is shown in Fig. 2. From Fig. 2a–d the values of ε' and ε'' both increase with temperature, and the intersection frequency shifts towards the higher frequency side as temperature increases. The values of ε' and ε'' at the intersection frequency (316 Hz) at a temperature of 383 K are approximately 525 (Fig. 2a). As the temperature increases to 423 K, ε' increases to 655, whereas ε'' increases to 1000, and they intersect at a frequency 575 Hz. With further increase in temperature up to 493 K, both ε' and ε'' values are increased sharply. The sharp rise of ε' and ε'' at low frequencies is most probably due to the effect of space charge polarization and/or conducting ion motion. It is observed that the dispersion in ε'' is stronger than that in ε', implying that it is influenced by dc conductivity. In the conducting dielectric materials, high ε'' values at a low frequency may be due to free charge motion within the material and are connected to ac conductivity relaxation.[17] Further studies of this phenomenon will be carried out by using the dielectric modulus formalism which suppresses the effect of electrode polarization or mobile ion polarization.

The temperature dependence of the dielectric constant (ε') at different frequencies for PCT ceramics is given in Fig. 3. It is observed that the

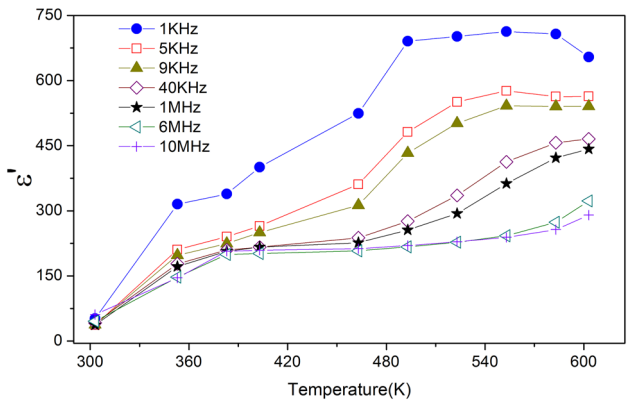

Fig. 3. Temperature dependence of dielectric constant at various frequencies of Pr_2CuTiO_6.

dielectric constant increases slowly with increasing temperature and a significant increase is observed at a critical temperature. The dielectric constant decreases with an increase in frequency and the critical temperature increases with increasing measuring frequency. This can be interpreted in the light of the strong correlation between the conduction mechanism and the dielectric behavior in the PCT ceramics.[18]

The dissipation factor, called loss tangent ($\tan\delta$), is a parameter of a dielectric material that quantifies its inherent dissipation of electric energy. The dielectric loss factor relates to the inability of dipoles in the material to reorient themselves with an alternating electric field. Figure 4 shows the temperature dependence of tangent loss ($\tan\delta$) at

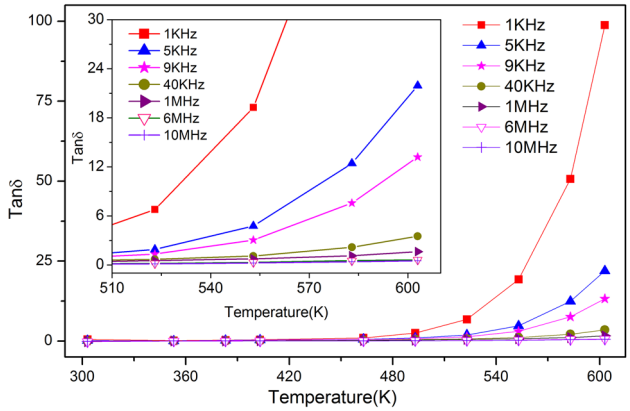

Fig. 4. Temperature dependence of tangent loss at various frequencies of Pr_2CuTiO_6.

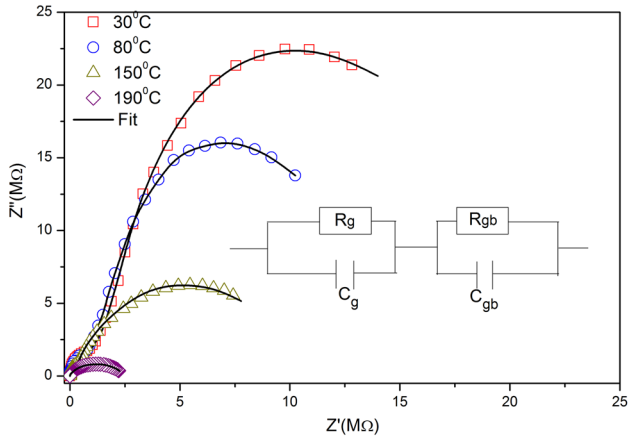

Fig. 5. Complex impedance plane plots of Pr_2CuTiO_6 at temperatures ranging from 30–150°C.

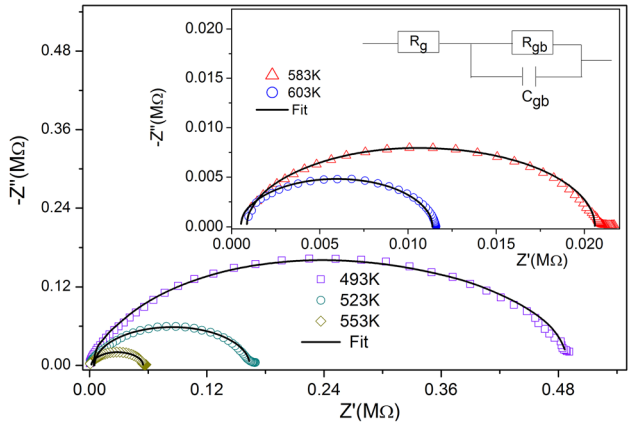

Fig. 6. Complex impedance plane plots of Pr_2CuTiO_6 at temperatures ranging from 220–320°C.

various frequencies for PCT compound. It can be seen that tanδ increases with increasing temperature, ensuring the semiconducting behavior which characterizes the dielectric perovskite. A sharp increase in the loss factor is observed with increase in temperature as a result of the strong conductivity contribution to tanδ. The increase in temperature thermally activates the charge carriers, increasing the charge carriers' exchange interactions, thereby enhancing ε' and tanδ.

Impedance Studies

The motion of charges could occur in different ways such as long range or short range charge displacement, dipole re-orientation, space charge formation, etc. The impedance properties arise due to intragrain, intergrain and electrode polarisations. The complex impedance $Z^*(\omega)$ can be described by the following relation:

$$Z^*(\omega) = Z'(\omega) + jZ''(\omega) \quad (1)$$

where Z' and Z'' represent the real and imaginary parts of impedance, respectively.

In Figs. 5 and 6, the Nyquist diagrams (Z'' versus Z' plots) of PCT are plotted using impedance data for various representative temperatures over a wide frequency range (100 Hz–1 MHz) in order to investigate the grain and grain boundary contributions to the electrical resistivity. Due to the dielectric relaxation from ideal Debye behaviour, Z^* plots for dielectric materials do not always give perfect or semicircular arcs. In this case, it is observed that all the semicircles exhibit a depression instead of a semicircle centered on the real axis (Z'). As semicircles of the PCT compound at different temperature are of a depressed type, non-Debye types of relaxations are suggested in which a distribution of relaxation times exist. Also, it has been noticed that in the temperature range 303–463 K, two depressed semicircular arcs are observed corresponding to grain and grain boundaries (Fig. 5), and single depressed semicircular arcs appear in the temperature range from 493 K to 603 K (Fig. 6). Each semicircular arc is modelled in terms of an electrical equivalent circuit consisting of a parallel combination of resistors and capacitors as shown in the insets in Figs. 5 and 6. The values of bulk resistance (R_g) and grain boundary resistance (R_{gb}) at different temperatures have been obtained from the intercept of the semicircular arcs on the Z' axis, and corresponding grain capacitance (C_g) and grain boundary capacitance (C_{gb}) values are calculated. It clearly shows that the parameters R_g and R_{gb} decrease with a rise in temperature, suggesting the negative temperature coefficient of resistance behavior of the material. The grain resistance (R_g), grain boundary resistance (R_{gb}) and grain boundary capacitance (C_{gb}) values at various temperatures are given in Table I. We have fitted our experimental data with equivalent electrical equations[19] for the grain and grain boundary as shown by solid lines in Figs. 5 and 6.

The frequency dependence of Z' of PCT at various temperatures is shown in Fig. 7. It is observed that Z' values decrease with a rise in temperature at low

Table I. Equivalent circuit parameters derived from the impedance plane plot for PCT

Temp (K)	R_g (MΩ)	R_{gb} (MΩ)	C_g (pF)	C_{gb} (pF)
303	5.64785	20.0000	53.2972	125.185
353	0.78228	11.06535	96.6555	156.542
423	0.48086	10.61930	108.7876	163.113
463	0.01596	2.33673	143.0821	155.144
493	0.00651	0.49408	–	127.290
523	0.00732	0.17286	–	120.478
553	0.00240	0.056243	–	122.610
583	0.00249	0.020992	–	102.777
603	0.00467	0.011665	–	77.9277

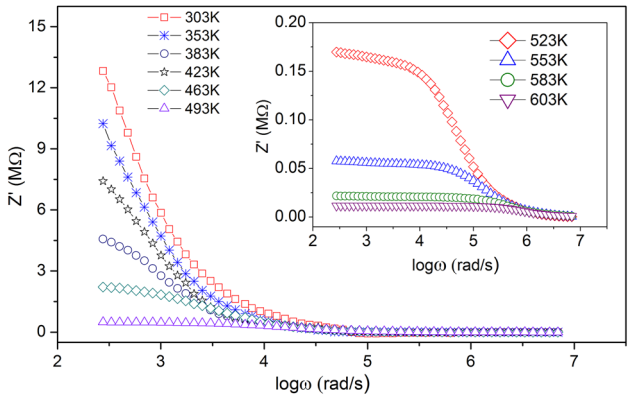

Fig. 7. Frequency dependence of real (Z') parts of impedance of Pr_2CuTiO_6 at various temperatures.

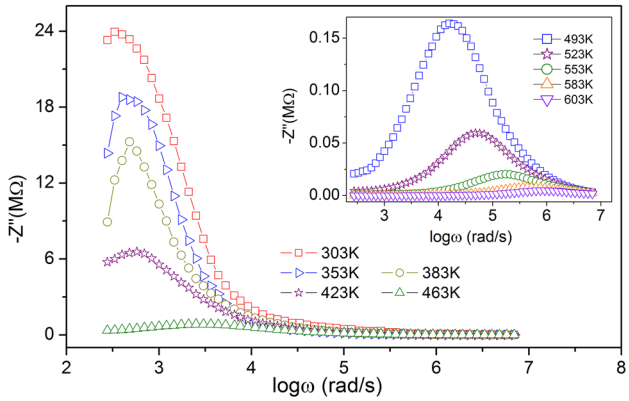

Fig. 8. Frequency dependence of imaginary (Z') parts of impedance of Pr_2CuTiO_6 at various temperatures of Pr_2CuTiO_6.

frequency, indicating increase in the ac conductivity in PCT. The values of Z' merge at a higher frequency region for all temperatures, implying the possible disappearance of space charges as a result of reduction in the barrier properties of the material. Figure 8 shows the frequency dependence of Z'' of PCT at various temperatures. The value of Z'' attains a maximum at a certain frequency (Z''_m) which indicates the presence of relaxation in the sample. The peak maxima (Z''_m) shifts to higher

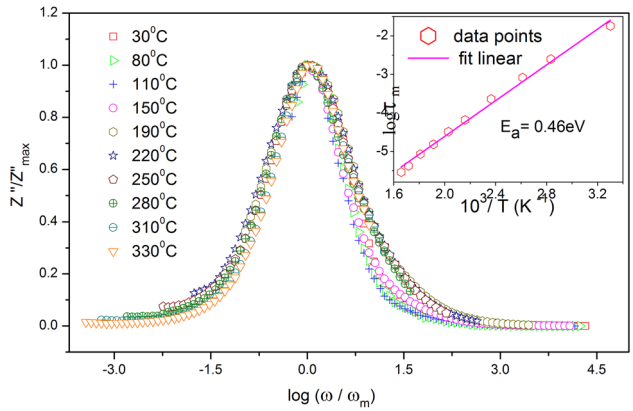

Fig. 9. Scaling behaviour of Z'' at various temperatures of Pr_2CuTiO_6. The temperature dependence of the most probable relaxation frequency is shown in the inset where the symbols are the experimental points and the solid line is the least squares straight line fit.

frequency regions with rising temperature, indicating that the resistance of the bulk material is decreasing and a strong dispersion of Z'' exists. The frequency at which Z'' attains its maximum value is known as the relaxation frequency. Again, an increase of relaxation frequency with rise in temperature suggests the temperature dependence of the relaxation phenomena in the material. The relaxation process occurs due to the presence of immobile charges at low temperatures and defects/oxygen vacancies at higher temperatures.[20]

The scaling behaviour of Z'' at various temperatures of Pr_2CuTiO_6 is shown in Fig. 9. The $Z''(\omega, T)/Z''_{max}$ versus log (ω/ω_m) plot shows that all curves collapse into one master curve, which indicates that the relaxation mechanism is nearly temperature-independent. A plot of the log τ_m versus inverse of absolute temperature ($1/T$) is shown in the inset of Fig. 9, where the circles are the experimental data and the solid line is the least squares straight line fit. The activation energy E_a calculated from the least squares fit to the points is 0.46 eV and relaxation time is $\tau_{0,m} = 1.5 \times 10^{-9}$s. The grain boundary resistance R_{gb} along with their relaxation frequencies ($\omega = 1/\tau$) are plotted in the form of an Arrhenius plot in Fig. 10. At all temperatures, R_{gb}

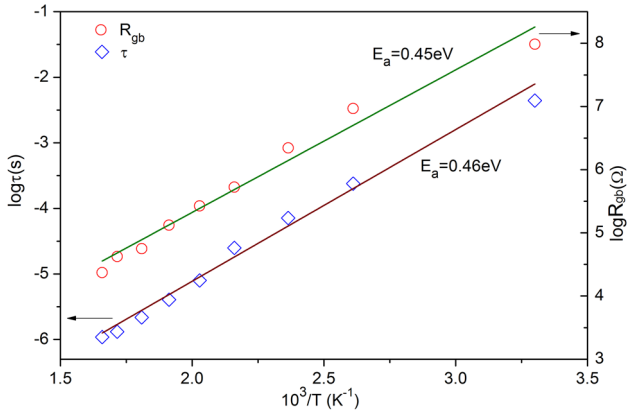

Fig. 10. Arrhenius plot for grain boundary resistance and relaxation time derived from the complex impedance plot.

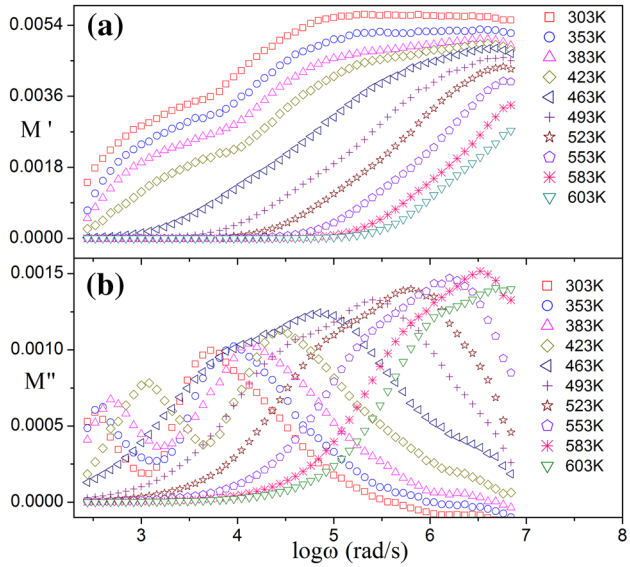

Fig. 11. Frequency dependence of (a) M' and (b) M'' of Pr_2CuTiO_6 at various temperatures.

and relaxation frequencies give a linear Arrhenius plot with activation energies of 0.45 eV and 0.46 eV, respectively. The grain boundary relaxation frequencies are obtained from the maxima of the semicircles in Nyquist diagrams (Z'' versus Z' plots) of PCT and used for calculation of activation energy of grain boundaries. The activation energy calculated using the grain boundary resistance data (0.45 eV) and their relaxation frequency (0.46 eV) is almost equal. Comparing the grain boundarie's activation energy (0.45 eV) with the activation energy (0.46 eV) calculated from the frequency dependence imaginary part of the resistance (Fig. 8) implies that the grain boundarie's resistances are the dominating characteristics for the overall electrical behavior of the material.

Electric Modulus Studies

Figure 11a and b shows the real and imaginary parts of the electric modulus, M' and M'', respectively, as a function of frequency at various temperatures. From Fig. 11a, it is clear that M' reaches a constant value at high frequencies at the end of the spectrum. At low frequencies, M' approaches zero, confirming the presence of an appreciable electrode and/or ionic polarization in the studied temperature ranges. M' increases from the low frequency of zero toward a high frequency limit, and the dispersion shift to the high frequency with increasing temperature may be due to the conductivity relaxation and short-range mobility of the charge carrier. At lower temperature regions (303–423 K), the trend of M' curves reveals the presence of two plateaus which can be attributed to two polarization effects. At higher temperatures (at and above 463 K), only one plateau is present on the M' curves due to the presence of only one polarization effect.

Figure 11b, which represents the variation of the imaginary part of the electrical modulus M'' with frequency at different temperatures, evidences the presence of two dielectric relaxations at lower temperatures (303–423 K) but only one at higher temperatures (at and above 463 K). These two dielectric relaxations indicate the contribution of both the grain and the grain boundary in the conductivity process. Further, the low-frequency side of the peak represents a range of frequency in which charge carriers can perform hopping from one site to their neighbouring sites. The high-frequency side of the peak represents a range of frequency in which charge carriers are spatially confined in their potential well and thus cannot make localized motion inside the well.[21] The shift of ghe peaks to higher frequencies with increasing temperature indicates the transition from short-range to long-range mobility with decreasing frequency.

The Argand diagram for the electric modulus (M'' versus M') of Pr_2CuTiO_6 at several temperatures is shown in Fig. 12. In order to confirm the ambiguity arising due to the presence of grain/grain boundary effect[22] at elevated temperatures, the impedance data are re-plotted in the modulus formalism. It is clear that the modulus plane plots exhibit two semicircles of unequal sizes between the temperature range of 303–423 K: one corresponds to grain and the other to grain boundary. Above 423 K, only one semicircle is observed which corresponds to the grain boundary contribution. This supports the behavior observed in Fig. 11b.

The normalized imaginary part of impedance Z''/Z''_{max} and the electric modulus M''/M''_{max} as a function of frequency at different temperatures can be seen in Fig. 13. The existence of an expected separation region between normalized Z″ and M″ variation with frequency is an evidence of local conduction and displacement from an ideal Debye behavior.[23–26] However, the peak frequency $\omega_{m''}$ in the M''/M''_{max} curve is shifted to a higher frequency

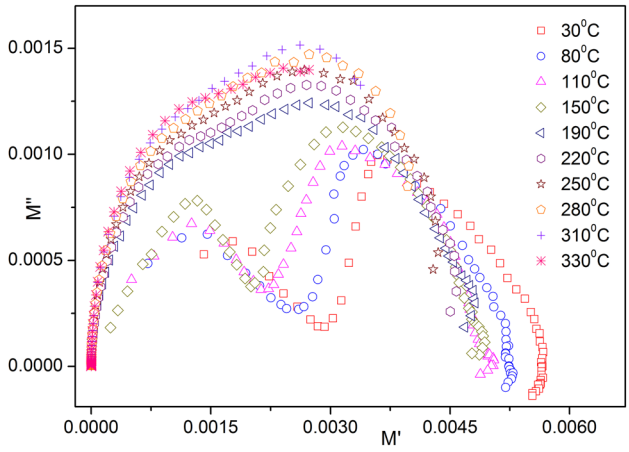

Fig. 12. Argand diagram for electric modulus (M' versus M'') of Pr_2CuTiO_6 at various temperatures.

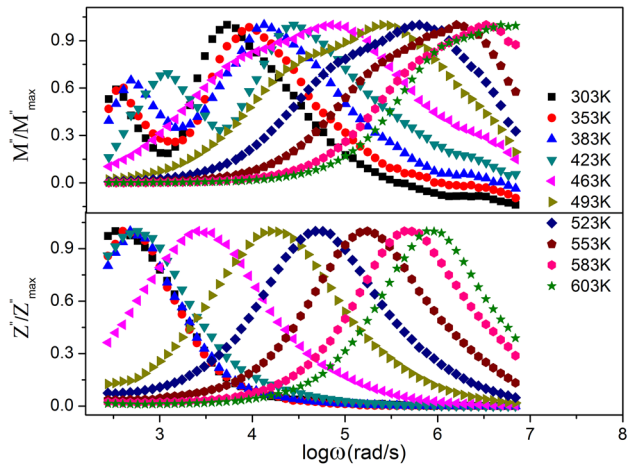

Fig. 13. Normalized imaginary part of impedance (Z') and normalized imaginary part of modulus (M') as a function of frequency at various temperatures for Pr_2CuTiO_6.

region with respect to $\omega_{m'}$ in the Z''/Z''_{max} curve. From the magnitude of mismatch between the peaks of both parameters, it is possible to observe a change of the apparent polarization.[24,27] The overlapping peak position of the Z''/Z''_{max} and M''/M''_{max} curves is interpreted as evidence of delocalized, long-range relaxation. Here, for our present system, the Z''/Z''_{max} and M''/M''_{max} peaks do not completely overlap but are instead very close, suggesting contributions from both long-range and localized relaxation effects. The comparison of the impedance and modulus data allows us to rationalize the bulk response in terms of localized (dielectric relaxation) and delocalized (ionic conductivity) relaxation processes.

Ac Conductivity

The alternative current (AC) conductivity σ_{ac} of various types of materials as a function of angular frequency ω is approximated by a 'universal power

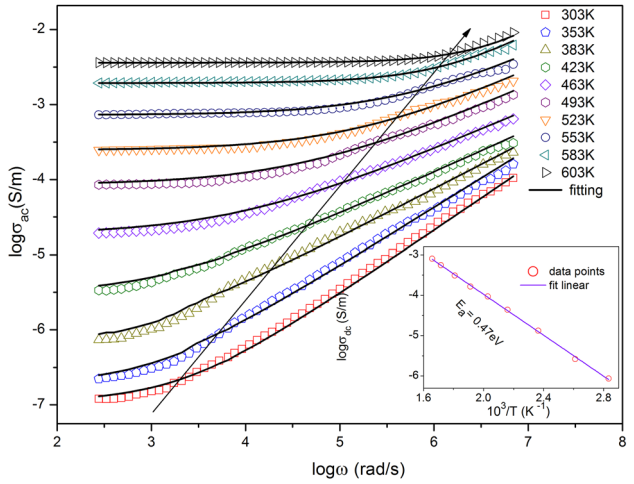

Fig. 14. Double logarithmic plot of ac conductivity versus frequency at several temperatures for Pr_2CuTiO_6. The left side of the arrow line represents dc conductivity and right side the frequency-dependent ac conductivity.

law' and reported by many investigators.[28–31] Figure 14 shows the variation of AC conductivity (σ_{ac}) as a function of frequency at different temperatures of Pr_2CuTiO_6 compound. From these curves, it is clear that the ac conductivity decreases with decreasing frequency and becomes almost frequency-independent at lower frequency region. Therefore, the AC conductivity spectra can be divided into two parts[30] as indicated by an arrow. In the first part, at a lower frequency region, a frequency-independent ac conductivity behaviour (plateau region) is observed for each temperature. In the plateau region, the conductivity $\sigma(0)$ increases with temperature showing that the conduction process is thermally activated. In the second part (i.e. right side of arrow line), the dispersion region corresponding to the high frequency part of the conductivity is observed. At higher frequencies, σ_{ac} increases because of the contribution of polarons,[30,31] which are moving from a localized site to another one in the material. The increase in σ_{ac} at higher frequencies is attributed to the charge motion in different regions of the material which supports the presence of isolated polarons in these regions.[30] A sharp increase of AC conductivity at high frequencies obeys Jonscher's power law equation[32]:

$$\sigma = \sigma_{dc}\left[1 + \left(\frac{\omega}{\omega_H}\right)^n\right] \quad (2)$$

where, ω_H is the hopping frequency of charge carriers with a change in its slope governed by the dimensionless frequency exponent n. According to Jonscher's power law, the origin of the frequency dependence of conductivity lies in the relaxation phenomena arising from mobile charge carriers. The experimental conductivity data of PCT are fitted to Eq. 2 with direct current conductivity σ_{dc}

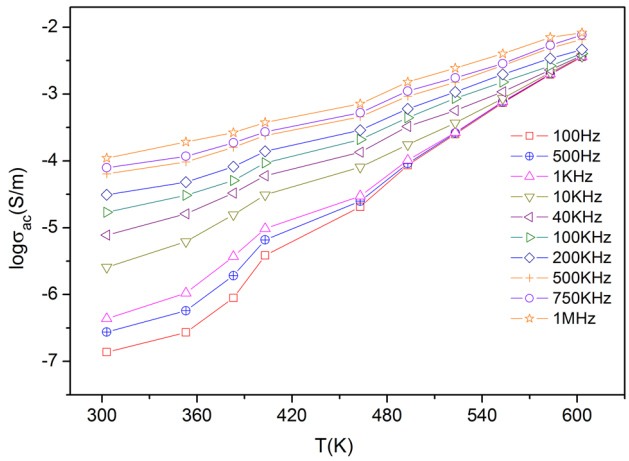

Fig. 15. Temperature dependence of ac conductivity for Pr_2CuTiO_6 at various frequencies (100 Hz–1 MHz).

and ω_H as variables keeping in mind that the values of parameter n are weakly temperature-dependent. The best fit of conductivity spectra is shown by solid lines in Fig. 14 at various temperatures. The reciprocal temperature dependence of σ_{dc} is shown in the inset of Fig. 14 which follows Arrhenius' law with an activation energy of 0.47 eV. This value of activation energy is very close to that reported by us for Pr_2ZnZrO_6.[33] Such a value of activation energy also confirms that the conduction mechanism in PCT may be due to the hopping of small polaron.[33–37]

Figure 15 shows the temperature dependence of ac conductivity of Pr_2CuTiO_6 ceramics at various frequencies (100 Hz–1 MHz). For all frequencies, the ac conductivity increases with a rise in temperature, further confirming the semiconductive nature of Pr_2CuTiO_6 ceramics. It can be seen that in the low temperature region, there is a distinct dispersion in the values of conductivity. The dispersion in the values of conductivity decreases with a rise in temperature. This is probably due to the fact that the conductivity is intrinsic at these temperatures. The variation of σ_{ac} in the low temperatures range is much sensitive than that in the relatively high temperature range. With an increase in the temperature the charge carriers get thermally activated which increases the charge carriers' exchange interactions, thereby enhancing σ_{ac}.

CONCLUSIONS

A polycrystalline Pr_2CuTiO_6 (PCT) ceramic was prepared by the multi-step mixed oxide route. Dielectric, impedance and modulus characteristics have been studied in a wide range of frequencies and temperatures. XRD analysis of PCT showed the monoclinic crystal structure. The Cole–Cole plots of impedance in PCT ceramics suggest the relaxation to be non-Debye-type. Studies of dielectric and impedance parameters as a function of temperature and frequency showed the significant effect of grains and grain boundaries in the relaxation process. The grain boundary resistances are the dominating characteristics for the overall electrical behavior of the material. The increase in temperature enhances σ_{ac} through the charge carrier's exchange interactions. The comparable values of the activation energy of both conductivity and modulus spectra indicate that the relaxation and conductivity process may be attributed to similar types of charge carriers (hopping of small polarons).

ACKNOWLEDGEMENTS

Dev Kumar Mahato acknowledges the Directorate of Extramural Research & Intellectual Property Rights (ER & IPR), Defence Res & Dev Orgn (DRDO) of India for providing the financial support under Grant No. ERIP/ER/1406036/M/01/1566.

REFERENCES

1. D. Cruickshank, *J. Eur. Ceram. Soc.* 23, 2721 (2003).
2. S. Sonmezoglu, A. Arslan, T. Serin, and N. Serin, *Phys. Scr.* 84, 065602 (2011).
3. J. Yu, T. Ishikawa, Y. Arai, S. Yoda, M. Itoh, and Y. Saita, *Appl. Phys. Lett.* 87, 252904 (2005).
4. P.K. Jana, S. Sarkar, and B.K. Chaudhuri, *J. Phys. D Appl. Phys.* 40, 556 (2007).
5. P. Thongbai, T. Yamwong, and S. Maensiri, *Solid State Commun.* 147, 385 (2008).
6. Y.Q. Lin, X.M. Chen, and X.Q. Liu, *Solid State Commun.* 149, 784 (2009).
7. Y.Q. Lin and X.M. Chen, *Appl. Phys. Lett.* 96, 142902 (2010).
8. W.T. Fu and D.J.W. Ijdo, *J. Solid State Chem.* 178, 2363 (2005).
9. W. Wersing, *Curr. Opin. Solid State Mater. Sci.* 1, 715 (1996).
10. N. Floros, J.T. Rijssenbeek, A.B. Martinson, and K.R. Poeppelmeier, *Solid State Sci.* 4, 1495 (2002).
11. D. Choudhury, A. Hazarika, A. Venimadhav, C. Kakarla, K.T. Delaney, P.S. Devi, P. Mondal, R. Nirmala, J. Gopalakrishnan, N.A. Spaldin, U.V. Waghmare, and D.D. Sarma, *Phys. Rev. B* 82, 134203 (2010).
12. S.B. Reddy, K.M. Kant, K.P. Rao, M. Opel, and M.S. Ramachandra Rao, *J. Magn. Magn. Mater.* 303, 332 (2006).
13. M.R. Palacín, J. Bassas, J.R. Carvajal, and P. Gómez-Romero, *J. Mater. Chem.* 3, 1171 (1993).
14. P. Gómez-Romero, M.R. Palacín, N. Casañ, A. Fuertes, and B. Martínez, *Solid State Ion.* 67, 603 (1993).
15. W.Z. Yang, M.M. Mao, X.Q. Liu, and X.M. Chen, *J. Appl. Phys.* 107, 124102 (2010).
16. S. Sonmezoglu and O.A. Sonmezoglu, *Mater. Sci. Eng. C* 31, 1619 (2011).
17. M.P. Dasari, K.S. Rao, P.M. Krishna, and G.G. Krishna, *Acta Phys. Pol. A* 119, 387 (2011).
18. S.S. Ata-Allah, *J. Solid State Chem.* 177, 4443 (2004).
19. D.K. Mahato, A. Dutta, and T.P. Sinha, *Mater. Res. Bull.* 47, 4226 (2012).
20. A.K. Jonscher, *Nature* 267, 673 (1977).
21. J.S. Kim, *J. Phys. Soc. Jpn.* 70, 3129 (2001).
22. R.N.P. Choudhary, D.K. Pradhan, C.M. Tirado, G.E. Bonilla, and R.S. Katiyar, *Phys. Status Solidi B* 244, 2254 (2007).
23. M.A.L. Nobreand and S. Lanredi, *J. Appl. Phys.* 93, 5576 (2003).
24. R. Gerhardt, *J. Phys. Chem. Solids* 55, 1491 (1994).
25. M.J.S. Rocha, M.C.C. Filho, K.R.B. Theophilo, J.C. Denardin, I.F. Vasconcelos, E.B. Araujo, and A.S.B. Sombra, *Mater. Sci. Appl.* 3, 6 (2012).
26. C.C. Silva and A.S.B. Sombra, *Mater. Sci. Appl.* 2, 1349 (2011).

27. R. Richert and H. Wagner, *Solid State Ion.* 105, 167 (1998).
28. A.N. Papathanassiou, *J. Phys. D Appl. Phys.* 35, L88 (2002).
29. A.N. Papathanassiou, *J. Non-Cryst. Solids* 352, 5444 (2006).
30. N.S. Asık, R. Tas, S. Sönmezoglu, M. Can, and G. Cankaya, *J. Non-cryst. Solids* 356, 1848 (2010).
31. S. Senkul, R. Tas, S. Sonmezoglu, and M. Can, *Int. J. Polym. Anal. Charact.* 17, 257 (2012).
32. A.K. Jonscher, *Dielectric Relaxation in Solids* (London: Chelsea Dielectric Press, 1983).
33. D.K. Mahato and T.P. Sinha, *J. Mater. Sci. Mater. Electron.* 24, 43999 (2013).
34. C. Bharti, M.K. Das, A. Sen, S. Chanda, and T.P. Sinha, *J. Solid State Chem.* 210, 219 (2014).
35. C. Bharti, A. Sen, S. Chanda, and T.P. Sinha, *J. Alloys Compd.* 590, 125 (2014).
36. D.K. Mahato and T.P. Sinha, *J. Alloys Compd.* 634, 246 (2015).
37. D.K. Mahato, S. Saha, and T.P. Sinha, *J. Mater. Sci. Mater. Electron.* 27, 3845 (2015).